Geophysical Research Letters

RESEARCH LETTER
10.1029/2025GL115738

Key Points:

- Half-space fault models generate a spectrum of slip behavior arising from heterogeneity in friction properties
- Transitions in slip speed depend on both the absolute length scale of heterogeneity and the ratio of fault friction parameters (*a*/*b*)
- Smaller scales of heterogeneity promote slow slip, whereas larger scales result in a sharper transition to unstable slip (earthquakes)

Supporting Information:

Supporting Information may be found in the online version of this article.

Correspondence to:

R. M. Skarbek,
rskarbek@psi.edu

Citation:

Skarbek, R. M., Saffer, D. M., & Savage, H. M. (2025). Not all heterogeneity is equal: Length scale of frictional property variation as a control on subduction megathrust sliding behavior. *Geophysical Research Letters*, *52*, e2025GL115738. https://doi.org/10.1029/2025GL115738

Received 7 MAR 2025
Accepted 14 APR 2025

Not All Heterogeneity Is Equal: Length Scale of Frictional Property Variation as a Control on Subduction Megathrust Sliding Behavior

Rob M. Skarbek[1], Demian M. Saffer[2,3], and Heather M. Savage[4]

[1]Planetary Science Institute, Tucson, AZ, USA, [2]Jackson School of Geosciences, Institute for Geophysics, University of Texas at Austin, Austin, TX, USA, [3]Department of Earth and Planetary Sciences, Jackson School of Geosciences, University of Texas at Austin, Austin, TX, USA, [4]Earth & Planetary Sciences, University of California Santa Cruz, Santa Cruz, CA, USA

Abstract Heterogeneity in geometry, stress, and material properties is widely invoked to explain the observed spectrum of slow earthquake phenomena. However, the effects of length scale of heterogeneity on macroscopic fault sliding behavior remain underexplored. We investigate this question for subduction megathrusts, via linear stability analysis and quasi-dynamic simulations of slip on a dipping fault characterized by rate-and-state friction. Frictional heterogeneity is imposed through alternating velocity-strengthening and velocity-weakening (VW) patches, over length scales spanning from those representative of basement relief (several km) to the entrainment of contrasting lithologies (100s of m). The resulting fault behavior is controlled by: (a) the average frictional properties of the fault, and (b) the size of VW blocks relative to a critical length scale. Reasonable ranges of these properties yield sliding behaviors spanning from stable sliding, to slow and seismic slip events that are confined within VW blocks or propagate along the entire fault.

Plain Language Summary Faults can slip at speeds ranging from tectonic plate rates to earthquakes, but we do not know why some faults seem more prone to slip faster or slower than others. One idea is that irregularities along the fault (possibly from fault geometry or the mixing of different rock types) could cause the fault to slip at different speeds. We test this idea using computer models of faults where we vary fault friction (resistance to sliding) on a fault broken up into patches with different frictional properties. Our results show that both the magnitude in the difference in frictional properties and the size of the patches are important in determining slip style.

1. Introduction

Over the past two decades, the discovery of a broad spectrum of slip behaviors on subduction megathrusts—and in other geologic settings—has ignited one of the most dynamic research fields in modern seismology and geodesy, focused on understanding the mechanisms that underlie varied modes of fault slip, and the window that these observations may provide into the physics of earthquakes and faulting (e.g., Beroza & Ide, 2011). Proposed mechanisms explaining this spectrum of slip behavior are numerous, and include frictional properties that vary with sliding velocity (e.g., Im et al., 2020; Shibazaki & Shimamoto, 2007), elevated pore pressure and concomitant low effective stress that promotes conditional stability (Liu & Rice, 2007), dilatant hardening that suppresses rapid slip once instability initiates (Liu & Rubin, 2010; Segall et al., 2010), and heterogeneity in fault geometry or frictional properties (e.g., Skarbek et al., 2012; Wang & Bilek, 2014).

We focus on the role of heterogeneity, which has emerged as a promising and widely invoked control on the slip behavior of faults, particularly as a mechanism explaining emergent, transient, slow failure in the form of slow slip events (SSEs), low- and very-low-frequency earthquakes (LFE/VLFE), and non-volcanic tremor (e.g., Barnes et al., 2020; Saffer & Wallace, 2015; Wang & Bilek, 2014). Geological and geophysical observations from drilling and seismic imaging document variations in geometry, stress, and/or material properties along faults that are tied to SSEs (e.g., Barnes et al., 2020; Wang & Bilek, 2014). Numerical modeling studies also demonstrate that heterogeneity in frictional properties can promote a spectrum of slip modes (e.g., Ando et al., 2010; Dublanchet et al., 2013; Luo & Ampuero, 2018; Luo & Liu, 2019, 2021; Nakata et al., 2011; Skarbek et al., 2012; Yabe & Ide, 2017). These studies have highlighted systematic relationships between peak slip speed and both (a) the ratio of fault length characterized by rate-weakening (unstable) versus rate-strengthening (stable) behavior;

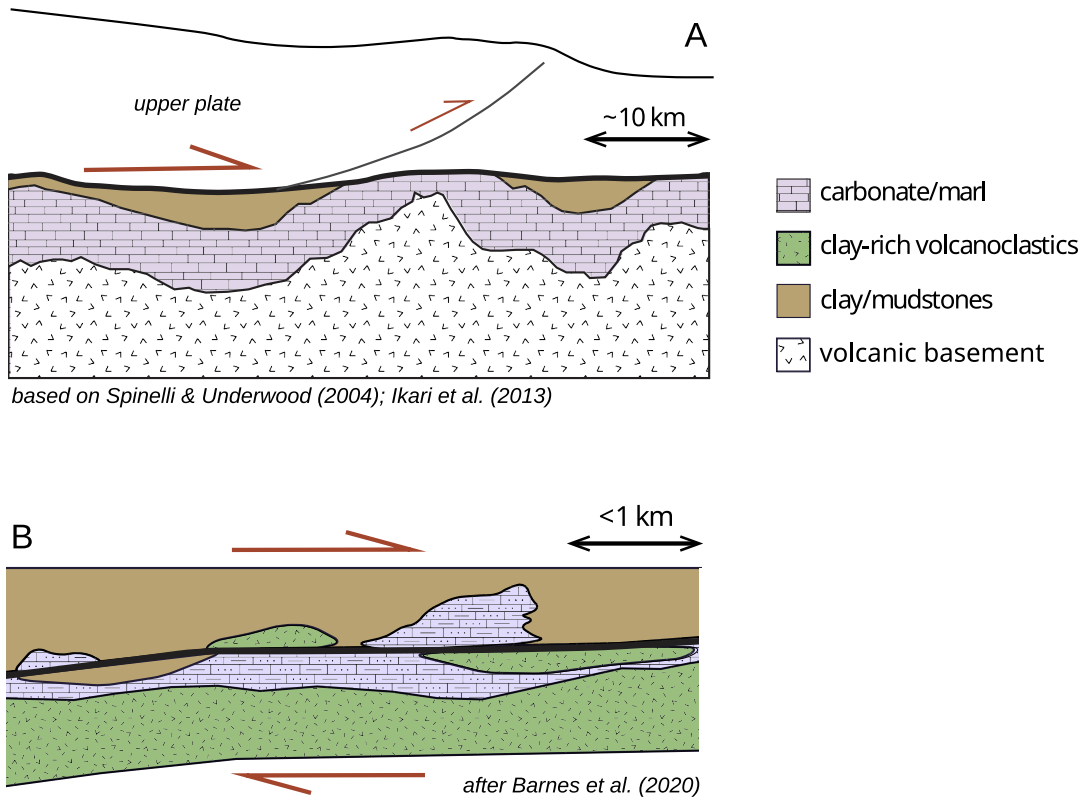

Figure 1. Schematic examples of scales and styles of lithological heterogeneity along the megathrust, rooted in observations at the (a) Costa Rica margin, where heterogeneity is linked to basement relief on the subducting Cocos Plate (e.g., Spinelli & Underwood, 2004), and (b) the Northern Hikurangi margin, where heterogeneity is linked to mixing and entrainment of contrasting lithologies along and within the megathrust fault zone (e.g., Barnes et al., 2020).

and (b) the magnitude of the rate strengthening versus rate weakening. However, the effect of the scale of heterogeneity on fault behavior has not received much attention.

Because the nucleation of instabilities requires a critical fault length/patch size that is dependent on frictional properties, stiffness, and normal stress (e.g., Scholz, 2019), it is natural to ask how the absolute scale of heterogeneity affects the mode and speed of fault failure, and whether small-scale heterogeneity leads to fundamentally different slip behavior than larger scale variations in frictional properties. This is of particular interest in understanding the origin and character of fault slip modes on natural faults, where heterogeneity manifests over a wide range of length scales (Figure 1). Here we investigate this question in the context of subduction megathrusts, through both linear stability analysis and a systematic set of quasi-dynamic numerical simulations of slip on a dipping fault that incorporate heterogeneity over a range of length scales, spanning from the scale of seamounts or basement relief (~10 km; e.g., Ikari, Niemeijer, et al., 2013; Kyriakopoulos & Newman, 2016), to the entrainment and mixing of lithologies along the fault zone (i.e., ~100 m scales or smaller) having different frictional properties (Figure 1; e.g., Barnes et al., 2020; Fagereng & Sibson, 2010).

2. Methods

We simulate sliding behavior on a dipping fault in an elastic half-space, with a geometry representative of an idealized subduction megathrust (Figure 2). For all of our simulations the fault has a nominal length $L = 100$ km; in detail, the fault length L_c for each simulation varies slightly due to numerical discretization to achieve specific sets of frictional properties and length scales of heterogeneity, as described below. The fault dips at an angle $\beta = 8°$ with its up-dip edge buried at a depth $d = 1$ km below an upper free surface. The effective normal stress σ_n' on the fault varies linearly with depth and is prescribed for a pore pressure ratio $(\lambda = P_{fluid}/\sigma_v)$ of 0.75, where P_{fluid} is fluid pressure and σ_v is lithostatic stress. This value of λ is representative of in situ fluid pressure estimates

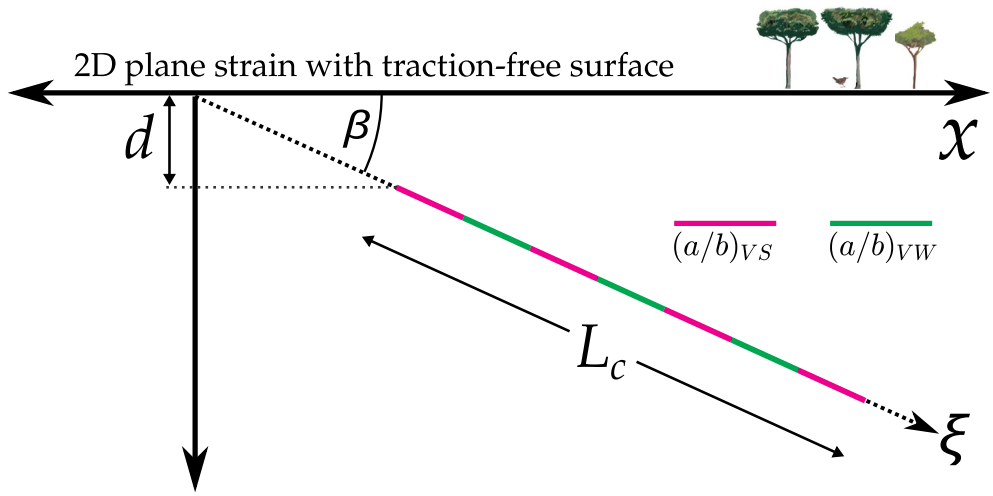

Figure 2. Model schematic. A fault of length L_c obeys rate and state friction. The fault dips at an angle β, and its up-dip edge is buried at a depth d below a traction-free surface. The fault is loaded by assuming steady sliding at $v_{plate} = 10^{-9}$ m/s along the black, dotted lines that are extensions of the fault along the ξ-axis (i.e., backslip loading).

at many subduction zones (e.g., Kitajima & Saffer, 2012; Saffer & Tobin, 2011), and results in an increase in σ_n' from ~2 MPa at the trench to ~30 MPa at the fault's down-dip edge. The fault is loaded by steady sliding at $v_{plate} = 10^{-9}$ m/s on extensions of the fault along the ξ-axis as defined in Figure 2 (i.e., backslip loading). The fault obeys rate and state friction (RSF), and we solve the equations governing fault motion using a quasi-dynamic boundary element code (see Text S1 in Supporting Information S1 for additional details; Skarbek, 2024).

Frictional heterogeneity is imposed on the fault by the inclusion of alternating velocity-strengthening (VS) and velocity-weakening (VW) blocks of lengths L_{VS} and L_{VW}, respectively (Figure 2; e.g., Luo & Ampuero, 2018; Skarbek et al., 2012; Yabe & Ide, 2017). Here, we refer to this type of model as a "block fault." The VS and VW sections of the fault and their respective lengths serve as an idealization of the lithologic changes and length scales that are illustrated in Figure 1. The fault begins and ends with a VS block, so that each VW block is loaded by slip on two adjacent VS sections.

The VS and VW sections are defined by values of the RSF parameters $(a - b)$ chosen to represent the properties of relevant materials along subduction megathrusts (e.g., Barnes et al., 2020; Ikari, Hüpers, & Kopf, 2013), and are directly constrained by laboratory experimental data for clay-rich (illite/quartz), (VS blocks; den Hartog et al., 2023), and carbonate gouges (VW blocks; Verberne et al., 2015). For simplicity, in this study we use constant values for each material, constrained by laboratory measurements at 150°C. To achieve these changes in $(a - b)$ we only vary the value of a, all other RSF parameters are constant (Table 1). For computational tractability, we assume $D_c = 8$ mm on the entire fault (Erickson et al., 2020, 2023), about an order of magnitude larger than values determined by den Hartog et al. (2023).

We characterize the frictional properties of the heterogeneous fault in terms of the fraction of the fault length that is velocity-weakening η and the mean value of (a/b) along the fault, which are linked via:

$$(a/b)_m = \eta(a/b)_{VW} + (1 - \eta)(a/b)_{VS}, \tag{1}$$

where $(a/b)_{VW}$ and $(a/b)_{VS}$ are values for the VW and VS blocks. Because the values of $(a/b)_{VS}$ and $(a/b)_{VW}$ are constant (i.e., the material properties are defined by lithology and thus are not free parameters), prescribing larger values of $(a/b)_m$ is accomplished by including fewer VW blocks of a given length (i.e., by decreasing η).

In reporting the length scale of the blocks, it is useful to define a normalized block length $\hat{L}_{VW} = L_{VW}/h_F^*$, where h_F^* is the theoretically defined critical perturbation wavelength for the velocity-weakening material

$$h_F^* = \frac{\pi G D_c}{\sigma_n'(1 - \nu)(b - a)_{VW}}, \tag{2}$$

Table 1
Symbols and Parameter Values

Parameter	Definition	Value and units
a_{VS}	RSF direct effect, VS material 150°C illite/quartz	0.0154
a_{VW}	RSF direct effect, VW material 150°C carbonate	0.0069
$(a/b)_m$	Average RSF rate parameter	0.89–1.35
b	RSF evolution effect	0.01
d	Up-dip burial depth	1 km
D_c	Characteristic state evolution distance	8 mm
G	Shear modulus	15 GPa
h_F^*	Critical wavelength for VW material using $\sigma_n' = 30$ MPa	6.1 km
L	Nominal fault length	100 km
L_b	Elasto-frictional length scale	601 m
L_c	Constructed fault length	93.7–108.9 km
L_{VS}	VS block length	300–4,866 m
L_{VW}	VW block length	120–14,087 m
v_0	RSF reference velocity	10^{-6} m/s
v_{plate}	Plate convergence rate	10^{-9} m/s
β	Fault dip angle	8°
η	Fraction of fault that is VW	0.22–0.77
λ	Pore pressure ratio	0.75
μ_0	Reference friction coefficient	0.3
ν	Poisson's ratio	0.35
σ_n'	Effective normal stress	2–30 MPa

where G is shear modulus, D_c is the RSF critical slip distance, and ν is Poisson's ratio (Rice & Ruina, 1983; Rice et al., 2001). We evaluate h_F^* using $\sigma_n' = 30$ MPa, corresponding to the fault's down-dip edge, along with the parameter values listed in Table 1.

For all of our simulations the spacing of numerical grid elements is $d\xi = L_b/20$, which is sufficient to resolve rupture fronts (e.g., Erickson et al., 2023), where $L_b = GD_c/\left[\sigma_n'(1-\nu)b\right]$. Because the fault is also discretized into VW and VS sections whose lengths L_{VW} and L_{VS} must be integer multiples of $d\xi$, the numerically constructed fault length L_c differs slightly from the nominal fault length L in some cases (see Text S1 in Supporting Information S1 for more details). To account for this effect, we only ran simulations for values of $(a/b)_m \leq 1.35$ that yield constructed fault lengths to within 10% of $L = 100$ km (Figure S1 in Supporting Information S1). The discretization also imposes limits on how precisely the value of $(a/b)_m$ can be controlled at small values of L_{VW}. Finally, the value of L_b for each simulation is evaluated using the value of σ_n' at the down dip edge of the numerical grid.

2.1. Linear Stability Behavior

We performed a linear stability analysis of the heterogeneous block fault system to guide the full simulations and develop insight into variations in sliding behavior and their underlying causes. Block fault models possess two linear stability modes that govern transitions in sliding behavior. There is a total instability (T-instability) mode mediated by $(a/b)_m$, in which the entire fault participates in unstable behavior (Dublanchet et al., 2013; Luo & Ampuero, 2018; Skarbek et al., 2012; Yabe & Ide, 2017). The T-instability boundary is governed by the average RSF values on the fault and is analogous to the stability boundary of a fault having constant frictional properties. This boundary occurs at $(a/b)_m = 1$, or $(a-b)_m = 0$.

There is also a partial instability (P-instability) mode governed by L_{VW}, where individual VW blocks become unstable once they reach a critical length L_{VW}^* that depends on the normal stress and RSF properties on both the

VW and VS sections of the fault (as noted in previous work; see Liu & Rice, 2007; Luo & Ampuero, 2018; Rubin, 2008; Yabe & Ide, 2017). Luo and Ampuero (2018) derived an equation for L^*_{VW} by analyzing a two-degree-of-freedom spring-slider system with periodic boundary conditions. Both the numerical simulations and linear stability results from Luo and Ampuero (2018) predict that the block fault becomes stable for any value of $(a/b)_m$ when L_{VW} is smaller than some minimum value $L^{\min}_{VW}$. However, this behavior as well as that predicted by their equation for L^*_{VW}, is qualitatively different from what we observe in our model (see Text S2 and Figure S2 in Supporting Information S1). The difference may be due to the fact that Luo and Ampuero (2018) studied a periodically repeating block fault in which the VW section was assigned to a single numerical cell. This allowed them to explore a large range of parameter space but enforced uniform slip in the VW section, whereas our model allows for slip gradients in the VW sections.

Instead of an analysis of a spring-slider model, we used a numerical method to perform a linear stability analysis of the same elastic continuum model that we used to perform our simulations (see Text S2 in Supporting Information S1; Skarbek, 2025). Thus, our linear stability results explicitly include the effects of finite fault length, variable effective stress, and the presence of a traction-free surface, as well as heterogeneous RSF properties. Using the parameter values in Table 1, the normalized critical VW block length for P-instability $\left(\hat{L}^*_{VW} = L^*_{VW}/h^*_F\right)$ depends on the value of $(a/b)_m$ and increases from 0.5 to about 0.55 as $(a/b)_m$ increases from 1 to 1.35 (Figure 3a). The partial and total instability boundaries intersect at $(a/b)_m = 1$ and $\hat{L}_{VW} = 0.5$, so that in the region defined by $(a/b)_m < 1$ and $\hat{L}_{VW} > 0.5$, both instability modes are active. Because the P-instability boundary depends on L_{VW}, the effect of different values of D_c (or $(a - b)$ or effective normal stress) can be anticipated by considering the scaled value L_{VW}/h^*_F.

2.2. Numerical Simulations

After determining the stability boundaries, we ran simulations of the full governing equations to determine the sliding behavior in the unstable region of our parameter space, and to examine how the peak sliding velocities $v_{\max}$ depend on the values of $(a/b)_m$ and $\hat{L}_{VW}$ (Figure 3a). We ran simulations until either consistent oscillations of maximum slip rate on the fault developed (i.e., a limit cycle), or the sliding velocity reached a uniform steady state such that $v(\xi, t) = v_{plate}$. We define $v_{\max}$ as the maximum velocity at any location on the fault during the time after one of these conditions was met. We also characterize the spatial uniformity of slip behavior on the fault by considering the ratio of $v_{\max}$ to the maximum sliding velocity $v^{VS}_{\max}$ at the centers of the VS sections, which represent the slowest sliding velocities along the fault (Figure 3b; e.g., Luo & Ampuero, 2018).

Following Abrahams et al. (2020), we define a "seismic" boundary where $v_{\max} > \sigma'_n(b - a_{VW})(1 - \nu)c/G \approx 1$ cm/s, with shear wave speed $c = 3500$ km/s and $\sigma'_n = 30$ MPa. We did not perform additional simulations within the seismic region beyond those necessary to determine the location of the boundary (yellow region in Figure 3a). We ran additional simulations in the stable region defined by $v_{\max} = v_{plate}$ (magenta region in Figure 3a) to confirm the boundaries defined by our linear stability analysis. We refer to simulations that produce periodic transient slip events with peak velocities below those in the seismic case as "slow" or "slow slip," defined by $v_{plate} < v_{\max} < 1$ cm/s.

3. Results

Regions of stable slip and seismic slip occur over large portions of our parameter space (magenta and yellow regions, respectively, in Figure 3a). The region between these two end members is defined by transient unstable slip with peak velocities below seismic slip speeds (<1 cm/s), representing a spectrum of fault slip behaviors. One fundamental result of our analysis is the definition of a finite region in parameter space that yields transient slow fault failure, clearly demonstrating that heterogeneity expands the conditions that produce emergent slow slip phenomena beyond a simple bifurcation at the stability threshold (e.g., Leeman et al., 2016). Consistent with previous work (Luo & Ampuero, 2018; Yabe & Ide, 2017) as well as simple theory, increased $(a/b)_m$ (i.e., an overall more VS fault) leads to more stable behavior (into the magenta region of Figure 3a). Our results also illustrate the importance of heterogeneity length scale on overall fault stability; for a given $(a/b)_m$, increasing block lengths leads to increasingly unstable behavior (Figures 3 and 4a).

Within the region of parameter space that produces slow slip, the scale of heterogeneity leads to systematic variations in behavior. Small scale heterogeneity ($L_{VW} < \sim 3$ km; $\hat{L}_{VW} < \sim 0.5$) and intermediate $(a/b)_m$ (from

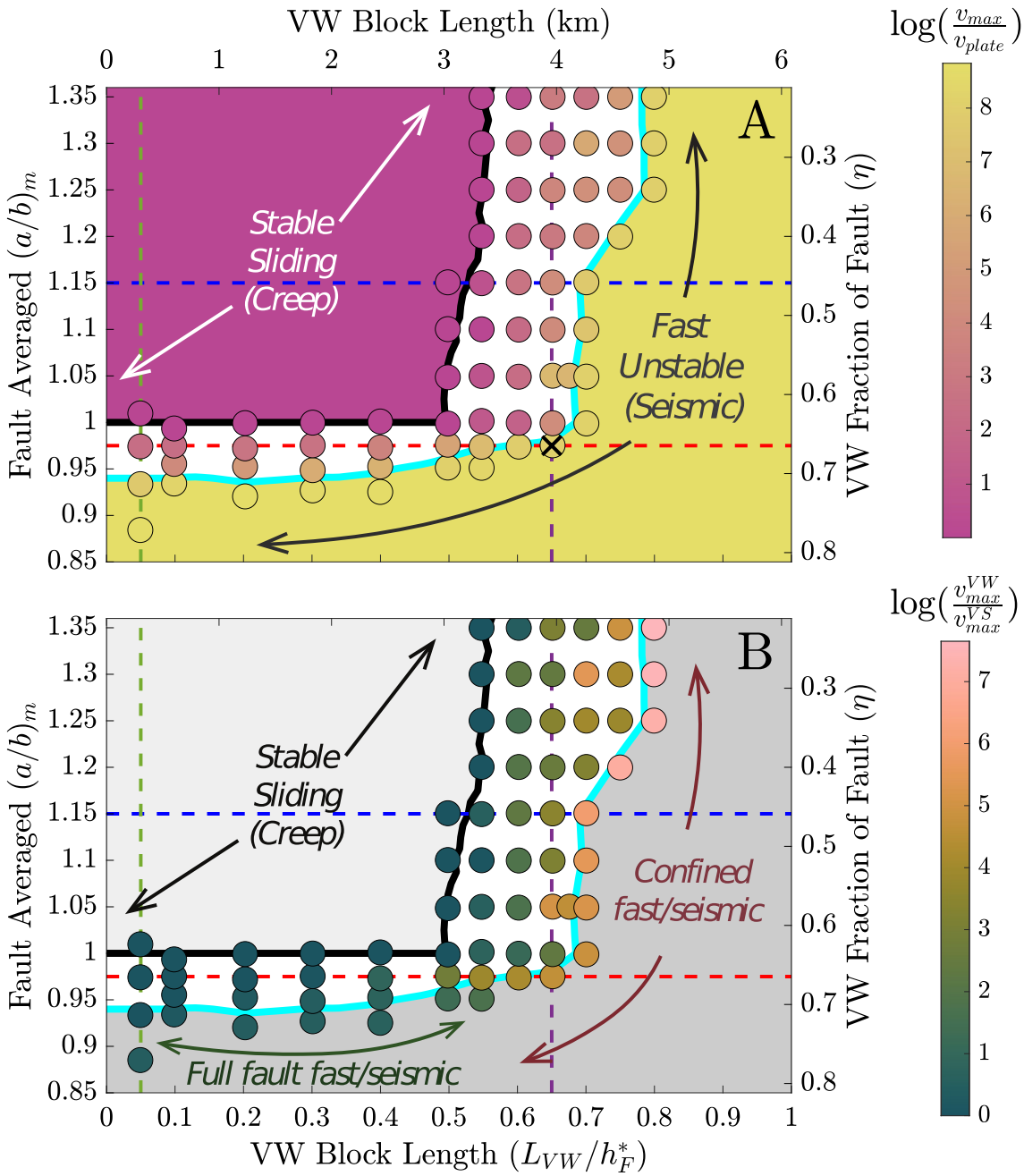

Figure 3. (a) Normalized maximum sliding velocity ($v_{\max}/v_{plate}$) on the fault for different values of $(a/b)_m$ and L_{VW}. Values of the fraction of the fault that is velocity-weakening (VW) (η) and dimensional VW block size are also shown. Each circle represents an individual simulation. The solid black line shows the stability boundaries determined as described in Section 2.1. The solid cyan line shows the seismic boundary defined by $v = 1$ cm/s, or $v/v_{plate} = 10^7$. The horizontal red and blue dashed lines correspond to the profiles of slip velocity and its dependence on VW block length plotted in Figure 4a, and the vertical green and purple lines correspond to those in Figure 4b showing the dependence of slip velocity on $(a/b)_m$. Movie S1 corresponds to the simulation marked with a black "X." (b) Contrast between maximum slip velocities on the entire fault and those at the centers of the velocity-strengthening sections ($v^{VS}_{\max}$).

~0.93 to 1) give rise to slow slip transients (red lines in Figures 3 and 4a). For the smallest scale of heterogeneity, the VW and VS blocks behave in unison, whereas for larger blocks ($L_{VW} > \sim 1.8$ km) slow slip prevails but with different slip speeds in the VW and VS blocks (Figure 3b). For more stable configurations overall ($(a/b)_m = 1.15$, blue lines in Figures 3 and 4a), the same slow slip behaviors emerge but only for block lengths larger than the critical length $\hat{L}^*_{VW} \approx 0.5$.

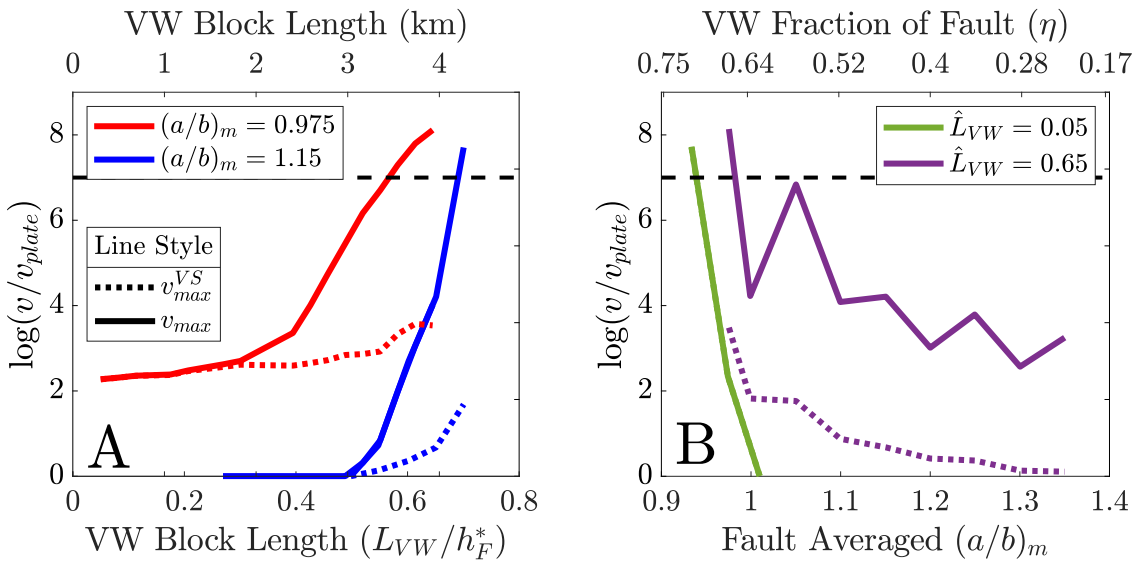

Figure 4. (a) and (b) Normalized maximum sliding velocity on the fault ($v_{\max}$, solid lines) and at the centers of the velocity-strengthening (VS) sections ($v_{\max}^{VS}$, dotted lines), for the profiles defined in Figure 3. In both panels the horizontal, dashed black line indicates the seismic velocity boundary ($v = 1$ cm/s, $v/v_{plate} = 10^7$). In panel B the values of $v_{\max}^{VS}$ and $v_{\max}$ overlie each other for $\hat{L}_{VW} = 0.05$ (green line), indicating that the entire fault slips at the same velocity.

This complexity is more pronounced at large scales of heterogeneity. For a wide range of friction behavior ($(a/b)_m$ up to and exceeding 1.35), slow slip and slow earthquake phenomena can occur (purple lines in Figures 3 and 4b). In these cases, the blocks are sufficiently large that the VS and VW blocks slip at different speeds (Figure 3b), yet the VW blocks are not sufficiently large or do not compose a large enough fraction of the fault surface to fail at seismic speeds (i.e., as confined seismic ruptures). In comparison, the VS blocks maintain the same speed as the VW blocks when the block sizes are small (green lines in Figures 3b and 4b).

4. Discussion and Conclusions

Our numerical linear stability analysis correctly predicts the value of L_{VW}^* and is confirmed by the full numerical simulation results. This is notable because the fault system is complicated - it has variable friction properties and normal stress and includes the effects of a traction-free surface. These are features that prevent the application of analytical techniques for linear stability analysis of elastic continuum models (e.g., Heimisson et al., 2019; Rice et al., 2001). Thus, the numerical stability analysis method should be useful for predicting the linear stability behavior for a wide range of fault systems and numerical models that cannot be investigated using analytical methods (Skarbek, 2025).

Our results show that the two features that determine the qualitative behavior of the block model are the average rate dependence of the fault $(a/b)_m$, and the length of the VW blocks relative to the critical block length L_{VW}^*. Depending on these values, a wide range of sliding behaviors can emerge, from stable sliding to slow and seismic slip events in which slip can be either spatially uniform or nonuniform. This spectrum of slow slip transients arises over a wide range of parameter space, and is not restricted to conditions that lie on or very close to the stability threshold as observed in the block fault model studied by Luo and Ampuero (2018) that assumed uniform slip in the VW section.

A fundamental result is that below a certain VW block length that depends on $(a/b)_m$, we expect the fault to behave with a single "effective friction behavior"—in which there is no difference in the slip behavior of the VW and VS blocks (also observed by Luo and Ampuero (2018)). This behavior encompasses cases of stable sliding, as expected from the stability boundaries (blue lines in Figures 3 and 4a), and also transient slow slip (red lines in Figures 3 and 4a). For our set of parameter choices, this uniform fault slip and effective friction behavior persists up to a VW block size of <1.8 km for slow slip behavior (red lines, Figure 4a), and <3 km for stable sliding (blue lines, Figure 4a). Because the value of $\hat{L}_{VW}$ scales with $1/h_F^*$, faults with low effective stress (high pore pressure) could contain heterogeneous blocks 10s of km in length and still slip in this "well-mixed" or apparently homogeneous fashion.

We find that non-uniform sliding emerges as the size of the VW blocks approaches L^*_{VW}. With increasing length scales of heterogeneity (L_{VW} increasing), the behavior of distinct blocks diverges but remains slow (sub-seismic)–until a point where seismic slip rates result (as confined ruptures) within VW blocks (Figures 3b and 4a). Non-uniform sliding is the primary style of slip in the regime characterized by slow transient slip events (Figure 3); in this regime the VS sections slip at most a few orders of magnitude above the loading rate (Figure 4). This confined rupture behavior is a potential mechanism to explain the co-occurrence of SSEs and small/micro earthquakes or tremor on faults. However, whether fast radiative events occur on the same fault surface as SSEs is an open subject (e.g., Bartlow, 2020; Nakano et al., 2018).

Additionally, the slip velocities in the VW sections are limited by the presence of the adjacent VS sections. As the length of the VS sections increases (i.e., $(a/b)_m$ increasing in Figure 4b), the peak slip velocities in both the VW and VS sections decrease. However seismic ruptures can still propagate along the fault by "jumping" between VW blocks (see Movie S1). Such behavior might be analogous to kinematic earthquake solutions that show patches of high moment release and complex source-time functions (e.g., Jia et al., 2022, 2023).

Our results offer insight into the slip behavior in subduction zones that have documented lithologic and geometric heterogeneity. For instance, the Hikurangi subduction zone fails in regular, large SSEs, although historic large earthquakes have occurred there as well (Wallace, 2020). The SSEs have been linked to mixing and entrainment of volcaniclastic rocks with slivers of carbonate, which introduces frictional heterogeneity on the scale of ∼1 km or less along the fault (Barnes et al., 2020). Such behavior indeed arises for small scales of heterogeneity in our models ($L_{VW} < \sim$2–3 km; Figure 3 and red lines in Figure 4a). We envision that the fault is behaving in the uniform failure mode described above, with velocity-weakening and velocity-strengthening blocks failing in SSEs at the same speed. This implies that compositional heterogeneity at length scales of meters up to several hundreds of meters should promote slow slip on large (tens of km dimension) coherent fault patches, as opposed to exclusively surrounding or associated with larger-scale features like seamounts (Bangs et al., 2023; Sun et al., 2020). However, regions in the vicinity of seamounts may host accompanying microseismicty or tremor in the upper plate, and/or related to superimposed variations in loading rate during SSEs. Conversely, the Costa Rican margin, where length scales of heterogeneity are on the order of 10 km or larger due to basement topography, exhibits behavior where patches fail in earthquake ruptures (∼M7) (DeShon et al., 2003; Kyriakopoulos & Newman, 2016; Norabuena et al., 2004; Protti et al., 1995). More generally, the larger the velocity-weakening blocks, the more we should expect large earthquakes and/or confined ruptures at a scale comparable to the size of these patches to be possible.

More broadly, our models provide a general framework for quantifying the interplay between the size of heterogeneities and their frictional properties in controlling the spectrum of observed fault slip behavior. Our analysis also shows that the incorporation of laboratory-derived friction values in realistic fault models (i.e., that include the effects of both heterogeneity and a free surface) allow a rich set of fault slip behaviors to emerge, without requiring a narrow range of conditions or frictional properties as is the case for paradigms derived from one degree of freedom spring-slider models.

Data Availability Statement

Simulation data and MATLAB scripts necessary for reproducing Figures 3 and 4 can be found at Zenodo (Skarbek et al., 2024). All of the numerical calculations in this paper were performed using a MATLAB package `RSFaultZ` available at https://github.com/rmskarbek/RSFaultZ (Skarbek, 2024). Files that can be used to automatically conduct all of the calculations are stored in the github repository directory: RSFaultZ/examples/blocks.

Acknowledgments
We thank Jenny Kroik for providing the happy little trees in Figure 2. This work was supported by NSF awards EAR-2319850 to RMS, EAR-2123255 and EAR-2319848 to DMS, and EAR-2319847 to HMS. Colors for Figure 3 were generated using a perceptually uniform color map (Crameri, 2019; Crameri et al., 2020).

References

Abrahams, L. S., Allison, K. L., & Dunham, E. M. (2020). Earthquake sequence dynamics at the interface between an elastic layer and underlying half-space in antiplane shear. *Journal of Geophysical Research: Solid Earth*, *125*(12), e2020JB020007. https://doi.org/10.1029/2020JB020007

Ando, R., Nakata, R., & Hori, T. (2010). A slip pulse model with fault heterogeneity for low-frequency earthquakes and tremor along plate interfaces. *Geophysical Research Letters*, *37*(10), L10310. https://doi.org/10.1029/2010GL043056

Bangs, N. L., Morgan, J. K., Bell, R. E., Han, S., Arai, R., Kodaira, S., et al. (2023). Slow slip along the Hikurangi margin linked to fluid-rich sediments trailing subducting seamounts. *Nature Geoscience*, *16*(6), 505–512. https://doi.org/10.1038/s41561-023-01186-3

Barnes, P. M., Wallace, L. M., Saffer, D. M., Bell, R. E., Underwood, M. B., Fagereng, A., et al. (2020). Slow slip source characterized by lithological and geometric heterogeneity. *Science Advances*, *6*(13), eaay3314. https://doi.org/10.1126/sciadv.aay3314

Bartlow, N. M. (2020). A long-term view of episodic tremor and slip in Cascadia. *Geophysical Research Letters*, *47*(3), e2019GL085303. https://doi.org/10.1029/2019GL085303

Beroza, G. C., & Ide, S. (2011). Slow earthquakes and nonvolcanic tremor. *Annual Review of Earth and Planetary Sciences*, *39*(1), 271–296. https://doi.org/10.1146/annurev-earth-040809-152531

Crameri, F. (2019). Scientific colour maps [Software]. *Zenodo*. https://doi.org/10.5281/ZENODO.1243862

Crameri, F., Shephard, G. E., & Heron, P. J. (2020). The misuse of colour in science communication. *Nature Communications*, *11*(1), 5444. https://doi.org/10.1038/s41467-020-19160-7

den Hartog, S. A. M., Marone, C., & Saffer, D. M. (2023). Frictional behavior downdip along the subduction megathrust: Insights from laboratory experiments on exhumed samples at in situ conditions. *Journal of Geophysical Research: Solid Earth*, *128*(1), e2022JB024435. https://doi.org/10.1029/2022JB024435

DeShon, H. R., Schwartz, S. Y., Bilek, S. L., Dorman, L. M., Gonzalez, V., Protti, J. M., et al. (2003). Seismogenic zone structure of the southern Middle America Trench, Costa Rica. *Journal of Geophysical Research: Solid Earth*, *108*(B10), 2491. https://doi.org/10.1029/2002JB002294

Dublanchet, P., Bernard, P., & Favreau, P. (2013). Interactions and triggering in a 3-D rate-and-state asperity model. *Journal of Geophysical Research: Solid Earth*, *118*(5), 2225–2245. https://doi.org/10.1002/jgrb.50187

Erickson, B. A., Jiang, J., Barall, M., Lapusta, N., Dunham, E. M., Harris, R., et al. (2020). The community code verification exercise for simulating sequences of earthquakes and aseismic slip (SEAS). *Seismological Research Letters*, *91*(2A), 874–890. https://doi.org/10.1785/0220190248

Erickson, B. A., Jiang, J., Lambert, V., Barbot, S. D., Abdelmeguid, M., Almquist, M., et al. (2023). Incorporating full elastodynamic effects and dipping fault geometries in community code verification exercises for simulations of earthquake sequences and aseismic slip (SEAS). *Bulletin of the Seismological Society of America*, *113*(2), 499–523. https://doi.org/10.1785/0120220066

Fagereng, Å., & Sibson, R. H. (2010). Mélange rheology and seismic style. *Geology*, *38*(8), 751–754. https://doi.org/10.1130/G30868.1

Heimisson, E. R., Dunham, E. M., & Almquist, M. (2019). Poroelastic effects destabilize mildly rate-strengthening friction to generate stable slow slip pulses. *Journal of the Mechanics and Physics of Solids*, *130*, 262–279. Retrieved from http://www.sciencedirect.com/science/article/pii/S002250961930239X

Ikari, M. J., Hüpers, A., & Kopf, A. J. (2013). Shear strength of sediments approaching subduction in the Nankai Trough, Japan as constraints on forearc mechanics. *Geochemistry, Geophysics, Geosystems*, *14*(8), 2716–2730. https://doi.org/10.1002/ggge.20156

Ikari, M. J., Niemeijer, A. R., Spiers, C. J., Kopf, A. J., & Saffer, D. M. (2013). Experimental evidence linking slip instability with seafloor lithology and topography at the Costa Rica convergent margin. *Geology*, *41*(8), 891–894. https://doi.org/10.1130/G33956.1

Im, K., Saffer, D., Marone, C., & Avouac, J.-P. (2020). Slip-rate-dependent friction as a universal mechanism for slow slip events. *Nature Geoscience*, *13*(10), 705–710. https://doi.org/10.1038/s41561-020-0627-9

Jia, Z., Jin, Z., Marchandon, M., Ulrich, T., Gabriel, A.-A., Fan, W., et al. (2023). The complex dynamics of the 2023 Kahramanmaraş, Turkey, Mw 7.8-7.7 earthquake doublet. *Science*, *381*(6661), 985–990. https://doi.org/10.1126/science.adi0685

Jia, Z., Zhan, Z., & Kanamori, H. (2022). The 2021 South Sandwich Island Mw 8.2 earthquake: A slow event sandwiched between regular ruptures. *Geophysical Research Letters*, *49*(3), e2021GL097104. https://doi.org/10.1029/2021GL097104

Kitajima, H., & Saffer, D. M. (2012). Elevated pore pressure and anomalously low stress in regions of low frequency earthquakes along the Nankai Trough subduction megathrust. *Geophysical Research Letters*, *39*(23), L23301. https://doi.org/10.1029/2012GL053793

Kyriakopoulos, C., & Newman, A. V. (2016). Structural asperity focusing locking and earthquake slip along the Nicoya megathrust, Costa Rica. *Journal of Geophysical Research: Solid Earth*, *121*(7), 5461–5476. https://doi.org/10.1002/2016JB012886

Leeman, J. R., Saffer, D. M., Scuderi, M. M., & Marone, C. (2016). Laboratory observations of slow earthquakes and the spectrum of tectonic fault slip modes. *Nature Communications*, *7*(1), 11104. https://doi.org/10.1038/ncomms11104

Liu, Y., & Rice, J. R. (2007). Spontaneous and triggered aseismic deformation transients in a subduction fault model. *Journal of Geophysical Research*, *112*(B9), B09404. https://doi.org/10.1029/2007jb004930

Liu, Y., & Rubin, A. M. (2010). Role of fault gouge dilatancy on aseismic deformation transients. *Journal of Geophysical Research: Solid Earth*, *115*(B10), B10414. https://doi.org/10.1029/2010JB007522

Luo, Y., & Ampuero, J.-P. (2018). Stability of faults with heterogeneous friction properties and effective normal stress. *Tectonophysics*, *733*, 257–272. Retrieved from https://www.sciencedirect.com/science/article/pii/S0040195117304596

Luo, Y., & Liu, Z. (2019). Rate-and-state model casts new insight into episodic tremor and slow-slip variability in Cascadia. *Geophysical Research Letters*, *46*(12), 6352–6362. https://doi.org/10.1029/2019GL082694

Luo, Y., & Liu, Z. (2021). Fault zone heterogeneities explain depth-dependent pattern and evolution of slow earthquakes in Cascadia. *Nature Communications*, *12*(1), 1959. https://doi.org/10.1038/s41467-021-22232-x

Nakano, M., Hori, T., Araki, E., Kodaira, S., & Ide, S. (2018). Shallow very-low-frequency earthquakes accompany slow slip events in the Nankai subduction zone. *Nature Communications*, *9*(1), 984. https://doi.org/10.1038/s41467-018-03431-5

Nakata, R., Ando, R., Hori, T., & Ide, S. (2011). Generation mechanism of slow earthquakes: Numerical analysis based on a dynamic model with brittle-ductile mixed fault heterogeneity. *Journal of Geophysical Research: Solid Earth*, *116*(B8), B08308. https://doi.org/10.1029/2010JB008188

Norabuena, E., Dixon, T. H., Schwartz, S., DeShon, H., Newman, A., Protti, M., et al. (2004). Geodetic and seismic constraints on some seismogenic zone processes in Costa Rica. *Journal of Geophysical Research: Solid Earth*, *109*(B11), B11403. https://doi.org/10.1029/2003JB002931

Protti, M., McNally, K., Pacheco, J., González, V., Montero, C., Segura, J., et al. (1995). The March 25, 1990 (Mw = 7.0, ML = 6.8), earthquake at the entrance of the Nicoya Gulf, Costa Rica: Its prior activity, foreshocks, aftershocks, and triggered seismicity. *Journal of Geophysical Research*, *100*(B10), 20345–20358. https://doi.org/10.1029/94JB03099

Rice, J. R., Lapusta, N., & Ranjith, K. (2001). Rate and state dependent friction and the stability of sliding between elastically deformable solids. *Journal of the Mechanics and Physics of Solids*, *49*(9), 1865–1898. Retrieved from http://www.sciencedirect.com/science/article/pii/S0022509601000424

Rice, J. R., & Ruina, A. L. (1983). Stability of steady frictional slipping. *Journal of Applied Mechanics*, *50*(2), 343–349. https://doi.org/10.1115/1.3167042

Rubin, A. M. (2008). Episodic slow slip events and rate-and-state friction. *Journal of Geophysical Research*, *113*(B11), B11414. https://doi.org/10.1029/2008JB005642

Saffer, D. M., & Tobin, H. J. (2011). Hydrogeology and mechanics of subduction zone forearcs: Fluid flow and pore pressure. *Annual Review of Earth and Planetary Sciences*, *39*(1), 157–186. https://doi.org/10.1146/annurev-earth-040610-133408

Saffer, D. M., & Wallace, L. M. (2015). The frictional, hydrologic, metamorphic and thermal habitat of shallow slow earthquakes. *Nature Geoscience*, *8*, 594–600. https://doi.org/10.1038/ngeo2490

Scholz, C. H. (2019). *The mechanics of earthquakes and faulting*. Cambridge University Press.

Segall, P., Rubin, A. M., Bradley, A. M., & Rice, J. R. (2010). Dilatant stregthening as a mechanism for slow slip events. *Journal of Geophysical Research*, *115*(B12), B12305. https://doi.org/10.1029/2010JB007449

Shibazaki, B., & Shimamoto, T. (2007). Modeling of short-interval silent slip events in deeper subduction interfaces considering the frictional properties at the unstable-stable transition regime. *Geophysical Journal International*, *171*(1), 191–205. https://doi.org/10.1111/j.1365-246X.2007.03434.x

Skarbek, R. M. (2024). rmskarbek/RSFaultZ: v1.0 [Software]. *Zenodo*. https://doi.org/10.5281/zenodo.10497312

Skarbek, R. M. (2025). The stability of frictional sliding on dip-slip and finite length faults. *Geophysical Journal International*, *241*(2), 826–839. https://doi.org/10.1093/gji/ggaf071

Skarbek, R. M., Rempel, A. W., & Schmidt, D. A. (2012). Geologic heterogeneity can produce aseismic slip transients. *Geophysical Research Letters*, *39*(21), L21306. https://doi.org/10.1029/2012GL053762

Skarbek, R. M., Saffer, D. M., & Savage, H. M. (2024). Not all heterogeneity is equal: Length scale of frictional property variation as a control on subduction megathrust sliding behavior. [Dataset]. *Zenodo*. https://doi.org/10.5281/zenodo.14269747

Spinelli, G. A., & Underwood, M. B. (2004). Character of sediments entering the Costa Rica subduction zone: Implications for partitioning of water along the plate interface. *Island Arc*, *13*(3), 432–451. https://doi.org/10.1111/j.1440-1738.2004.00436.x

Sun, T., Saffer, D., & Ellis, S. (2020). Mechanical and hydrological effects of seamount subduction on megathrust stress and slip. *Nature Geoscience*, *13*(3), 249–255. https://doi.org/10.1038/s41561-020-0542-0

Verberne, B. A., Niemeijer, A. R., De Bresser, J. H. P., & Spiers, C. J. (2015). Mechanical behavior and microstructure of simulated calcite fault gouge sheared at 20-600°C: Implications for natural faults in limestones. *Journal of Geophysical Research: Solid Earth*, *120*(12), 8169–8196. https://doi.org/10.1002/2015JB012292

Wallace, L. M. (2020). Slow slip events in New Zealand. *Annual Review of Earth and Planetary Sciences*, *48*(1), 175–203. https://doi.org/10.1146/annurev-earth-071719-055104

Wang, K., & Bilek, S. L. (2014). Invited review paper: Fault creep caused by subduction of rough seafloor relief. *Tectonophysics*, *610*, 1–24. Retrieved from http://www.sciencedirect.com/science/article/pii/S0040195113006896

Yabe, S., & Ide, S. (2017). Slip-behavior transitions of a heterogeneous linear fault. *Journal of Geophysical Research: Solid Earth*, *122*(1), 387–410. https://doi.org/10.1002/2016JB013132

References From the Supporting Information

Dieterich, J. H. (1992). Earthquake nucleation on faults with rate- and state-dependent strength. *Tectonophysics*, *211*(1–4), 115–134. https://doi.org/10.1016/0040-1951(92)90055-B

Lapusta, N., Rice, J. R., Ben-Zion, Y., & Zheng, G. (2000). Elastodynamic analysis for slow tectonic loading with spontaneous rupture episodes on faults with rate-and-state dependent friction. *Journal of Geophysical Research: Solid Earth*, *105*(B10), 23765–23789. https://doi.org/10.1029/2000JB900250

Okada, Y. (1992). Internal deformation due to shear and tensile faults in a half-space. *Bulletin of the Seismological Society of America*, *82*(2), 1018–1040. https://doi.org/10.1785/bssa0820021018

Rice, J. R. (1993). Spatiotemporal complexity of slip on a fault. *Journal of Geophysical Research: Solid Earth*, *98*(B6), 9885–9907. https://doi.org/10.1029/93JB00191

Rice, J. R., & Ben-Zion, Y. (1996). Slip complexity in earthquake fault models. *Proceedings of the National Academy of Sciences of the United States of America*, *93*(9), 3811–3818. https://doi.org/10.1073/pnas.93.9.3811

Viesca, R. C. (2016a). Self-similar slip instability on interfaces with rate- and state-dependent friction. *Proceedings of the Royal Society A: Mathematical, Physical and Engineering Sciences*, *472*(2192), 20160254. Retrieved from http://rspa.royalsocietypublishing.org/content/472/2192/20160254

Viesca, R. C. (2016b). Stable and unstable development of an interfacial sliding instability. *Physical Review E - Statistical Physics, Plasmas, Fluids, and Related Interdisciplinary Topics*, *93*(6), 060202. Retrieved from https://link.aps.org/doi/10.1103/PhysRevE.93.060202